RSC Advances

PAPER

View Article Online
View Journal | View Issue

Cite this: *RSC Adv.*, 2017, **7**, 31619

Hybrid Cu_xO–TiO_2 porous hollow nanospheres: preparation, characterization and photocatalytic properties†

Yingqiao Xiang,[a] Yingying Li,[b] Xintong Zhang,[b] Annan Zhou,[a] Nan Jing[a] and Qinghong Xu*[a]

Received 10th May 2017
Accepted 12th June 2017

DOI: 10.1039/c7ra05281b

rsc.li/rsc-advances

A series of Cu_xO–TiO_2 hollow nanospherical composites with different mass percents of copper were prepared by an impregnation method, and the TiO_2 hollow nanospheres were prepared by hydrolysis of tetraethoxy titanium on the surface of spherical SiO_2 nanoparticles and corrosion of SiO_2 in NaOH solution. Cu_xO–TiO_2 hollow nanospheres displayed higher photocatalytic activities towards acetaldehyde degradation to CO_2 than TiO_2@SiO_2 nanospheres and TiO_2 hollow nanospheres under UV and visible-light irradiation due to the narrowed band gap of TiO_2 and enhanced charge separation after copper was introduced. In particular, the Cu_xO–TiO_2 hollow nanospheres show high catalytic activities in degradation under visible-light irradiation.

1. Introduction

In the past decades, titanium dioxide (TiO_2) has attracted increasing attention due to its extensive application such as in sensor technology,[1,2] pigments,[3] solar cells,[4] self-cleaning coatings[5] and photocatalysis.[6,7] Particularly, study on the photocatalytic properties of TiO_2 is the most common because of its several advantages including low cost, innocuity, chemical stability and high refractive index.[8–11] However, there are some disadvantages in using TiO_2, such as small surface area, phase transition, crystal growth and low quantum efficiency, which limit the photocatalytic efficiency of the catalysts.[12–14]

In order to overcome these problems, many investigations have been reported.[15–17] Morphology control and preparation of titania-based materials are two very effectual strategies.[18] One of the most efficient ways is to coat TiO_2 in form of a layer on surface of core materials with high surface area, such as ZrO_2, MoO_3, Fe_2O_3 and SiO_2.[19,20] Silica is one of the best core materials for its well-known surface chemistry, absorption capacity, controllable preparation and it can be easily eliminated.[21] Another is to synthesize TiO_2 with different morphologies and microstructures to enhance the surface area of the semiconductor. Many new morphologies of TiO_2 were synthesized in the past years, such as nanotubes, nanorods, and hollow spheres, *etc.*[22] The synthesis of TiO_2 hollow nanosphere is especially concerned for its large surface area, low density, and high light-harvesting efficiency.[23,24]

Volatile organic compound is the sources of indoor air pollution, and it is always the central issues in the environmental protection field. Among various photocatalytic oxidations over semiconductors, TiO_2 photocatalyst possesses the function of air purification. Despite of good photocatalytic activities, TiO_2 is only effective to degrade some photosensitive organic compounds under ultraviolet (UV) irradiation with strong intensity. However, the intensity of UV-light from common filament lamp is below several $\mu W\ cm^{-3}$, which is one thousand times low to the sunlight.[25] So the catalyst cannot reach the desired effect to get rid of the indoor contaminated gases. Therefore, development of visible-light-sensitive photocatalysts based on TiO_2 is necessary.

Another, due to high prices and scarce of the noble metal, attention has been given to search an alternative catalytic component to replace the noble metal. Such as, copper or copper oxide is better substitute component because of their low cost and wide use. In 2009, TiO_2 powder grafted by Cu^+ ions was found to be sensitive to visible light by Irie and his co-workers,[26] which lighted up the hope to TiO_2 on its applications in daily life. They studied the photocatalytic activity of Cu/TiO_2 under visible light irradiation. Huang *et al.* prepared the CuO/TiO_2 by the deposition–precipitation (DP) and investigated its catalytic behavior.[27] Also, Gnanasekaran *et al.* did many research to expand the absorption of TiO_2 to the visible light range for improving the photocatalytic efficiency.[28,29] Although photocatalytic efficiency of TiO_2 is improved markedly, catalytic efficiency of the catalyst is still unsatisfying. Based on these works, we determine to use high specific surface area porous TiO_2 hollow spheres as the carrier of loading copper, and study their catalytic activities by degradation of acetaldehyde gas.

[a]*State Key Laboratory of Chemical Resource Engineering, Beijing University of Chemical Technology, Box. 98, 15 Beisanhuan Donglu, Beijing 100029, PR China. E-mail: xuqh@mail.buct.edu.cn; Fax: +86-10-64425385; Tel: +86-10-64425037*

[b]*Key Laboratory for UV-Emitting Materials and Technology of Ministry of Education, Northeast Normal University, 5268 Renmin Street, Changchun 130024, PR China*

† Electronic supplementary information (ESI) available. See DOI: 10.1039/c7ra05281b

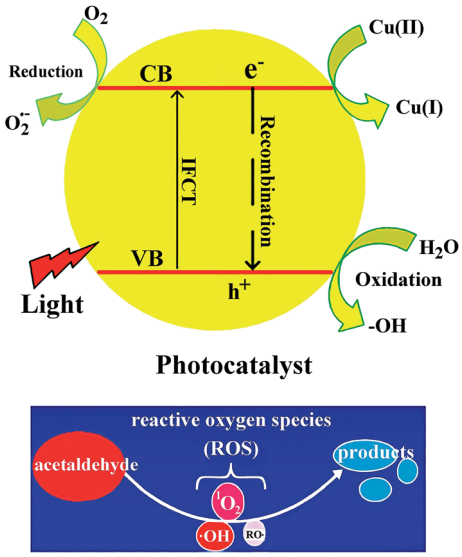

Scheme 1 Possible mechanism on degradation of acetaldehyde under the existence of $Cu_xO@TiO_2$ catalysts.

In this paper, $TiO_2@SiO_2$ core–shell nanosphere was prepared by using silica gel nanosphere as hard template, and TiO_2 hollow nanosphere was obtained after SiO_2 was etched by NaOH solution with a certain concentration. Cu^{2+} ions were adsorbed and Cu_xO was formed on the surface of the TiO_2 hollow nanosphere to enhance separation of the photo-generated charge carriers. Four kinds of photocatalysts, $TiO_2@SiO_2$ nanosphere, TiO_2 hollow nanosphere, Cu_xO–$TiO_2@SiO_2$ nanosphere and Cu_xO–TiO_2 hollow nanosphere, were synthesized. The catalytic activities of these catalysts were studied by degradation of acetaldehyde under UV and visible-light irradiations. The results indicate that all catalysts have good catalytic activities in degradation of acetaldehyde under UV-light irradiation, and the Cu_xO–TiO_2 hollow nanosphere shows high catalytic activities in the degradation under visible-light irradiation. As shown in Scheme 1, the visible-light is considered to initiate interfacial charge transfer. If the photon energy of light is greater than the semiconductor band gap, the electron (e^-) on the valence band will be excited to the conduction band and the hole (h^+) will be generated at the valence band. When Cu_xO–TiO_2 is used as photocatalyst, electrons in the valence band (VB) of TiO_2 are stimulated and directly transferred to Cu(II) to form Cu(I), as well as holes (h^+) in the VB of TiO_2. Also the adsorbed O_2 on the surface can capture the electrons in VB of TiO_2, but it is harder than that of Cu(II). Thus, the energy to separate electrons and holes becomes low, which narrows the band gap of TiO_2 and prolongs the absorption edge from UV-light to visible-light region. The holes produced in VB of TiO_2 decompose organic substances.

2. Experimental

2.1. Chemicals and instruments

All chemicals used are of analytical reagent grade available from a commercial supplier without further purification. Tetraethoxysilane (TEOS, ≥99%) and copper chloride dihydrate ($CuCl_2 \cdot 2H_2O$, AR) were purchased from Sinopharm Chemical Reagent Company (in Shanghai, PR China). Tetraethoxy titanium ($C_8H_{20}O_4Ti$, ≥98%) was purchased from Aladdin Industrial Corporation (in Shanghai, PR China). L-Lysine (BR) was purchased from Beijing Biological Technology Company (in Beijing, PR China). Hydrochloric acid (38 wt%), acetic acid (38 wt%), sodium hydroxide (AR) and ethanol (AR, 99%) were all purchased from Beijing Chemical Reagent Company (in Beijing, PR China).

Fourier transform infrared (FT-IR) spectra of the samples were recorded in range of 4000–400 cm^{-1} with 2 cm^{-1} resolution on a Bruker Vector-22 Fourier transform spectrometer (made in Germany). Electronic micrographs (including energy-dispersive X-ray spectroscopy, EDS) of the samples were observed using a S-4700 scanning electron microscope (SEM, made in Japan) operated at 15 kV, a J-2010 high resolution transmission electron microscope (HRTEM, made in Japan) and a Tecnai G^2 20S-TWIN transmission electron microscope (TEM, made in USA) operated at 200 kV, respectively. Crystal structures of samples were determined by powder X-ray diffraction (PXRD), using a Rigaku D/MAX diffractometer (made in Japan) with Cu Kα radiation (λ = 0.15406 nm, scanning speed = 10° min^{-1}). N_2 sorption isotherms of the samples were recorded on a Quantachrome NOVA 2000e sorption analyzer (made in USA) at the temperature of liquid nitrogen (77 K). Samples were degassed at 200 °C overnight prior to the measurement. Surface areas and pore size distributions of the samples were obtained by Brunauer–Emmett–Teller (BET) method and calculated using Barrett–Joyner–Halenda (BJH) model, respectively. UV-Vis absorption of the samples were obtained by Perkin Elmer Lambda 900 UV-Vis spectrophotometer (made in Germany) in range of 220–800 cm^{-1}. X-ray photoelectron spectroscopic (XPS) analysis was measured on Shimadzu ESCA-250 and ESCA-1000 spectrometers (made in Japan) with Mg K_α X-ray sources.

STEM analysis was conducted on a JEOL JEM 2200FS equipped with a CEOS aberration corrector (CEOS GmbH, Heidelberg, Ger). Images and EDS maps were acquired in analytical mode (AMAG), with a probe size of 0.8 nm and a nominal beam current of 450 pA. The EDS signal was collected with a Bruker X-Flash silicon-drift detector and was processed using the Bruker Esprit software. EDS maps were collected for >10 min. The final resolution of the EDS maps was estimated to be ~0.8 nm.

2.2. Synthesis of $TiO_2@SiO_2$ nanosphere

Silica nanosphere was used as template to synthesize TiO_2 hollow nanosphere, and its synthesis was according to the method in ref. 30.

$TiO_2@SiO_2$ with core–shell structure was composited *via* sol–gel method. Primarily, the as-prepared SiO_2 nanosphere with diameter about 25 nm was dispersed in an ethanol solution (ethanol in water) and oscillated in ultrasonic oscillator for several minutes. A solution of tetraethoxy titanium in ethanol was then added dropwise to 35 mL of the above dispersion system with continuous stirring. And a mixture solution of 35

mL of absolute ethanol, 2.0 mL acetic acid and two drops of hydrochloric acid was added to the mixture rapidly. After stirred for 30 min, the mixture was heated at 40 °C and stirred vigorously for 1.0 h. The final product TiO_2@SiO_2 nanosphere was obtained after the mixture was filtered, washed with water and ethanol for several times, dried at 70 °C for about 4.0 h and calcined at 550 °C for 4.0 h.

2.3. Synthesis of TiO_2 hollow nanosphere

The silica template was removed by immersing TiO_2@SiO_2 nanosphere in a NaOH solution (3.0 M) at 60 °C for 8.0 h under continuous stirring, and the hollow nanosphere was obtained after the mixture was centrifuged, washed with ethanol and water for several times and dried at 60 °C for 4.0 h.

2.4. Synthesis of Cu_xO–TiO_2 hollow nanosphere and Cu_xO–Ti–TiO_2@SiO_2 nanosphere

The Cu_xO–TiO_2 hollow nanosphere and Cu_xO–TiO_2@SiO_2 nanosphere were prepared by an impregnation method using $CuCl_2 \cdot 2H_2O$ as source of Cu^{2+} ions. 1.0 g of TiO_2 hollow nanosphere (or TiO_2@SiO_2 nanosphere) was added into 10 mL distilled water in a vial reactor. Different amounts of $CuCl_2 \cdot 2H_2O$ (mass percents of Cu^{2+} relative to TiO_2 are 0.25%, 0.50% and 1.0%, respectively) were added to the above reactor, and the system was heated at 90 °C for 1.0 h under continuous stirring. The products were obtained by centrifuged, washed with water for several times and dried at 110 °C overnight. The products are named as 0.25%-Cu_xO–TiO_2 hollow nanosphere, 0.5%-Cu_xO–TiO_2 hollow nanosphere and 1.0%-Cu_xO–TiO_2 hollow nanosphere, respectively; or 0.25%-Cu_xO–TiO_2@SiO_2 nanosphere, 0.5%-Cu_xO–TiO_2@SiO_2 nanosphere and 1.0%-Cu_xO–TiO_2@SiO_2 nanosphere, respectively.

2.5. Measurement of photocatalytic activities

Photocatalytic activities of the synthesized materials were evaluated by degradation of acetaldehyde in gas phase under ultraviolet and visible-light irradiations. 0.05 g microsphere powder was uniformly spread in a sample holder, which was placed on the bottom of a 500 mL cylinder-type Pyrex glass vessel. The glass vessel was flushed with O_2 (20%)/N_2 gas to remove carbon dioxide from the system, and the relative humidity of atmosphere inside the vessel was controlled to 45% by passing the O_2/N_2 gas through chilled water formerly. 5.2 mL acetaldehyde was introduced into the reaction vessel using a Pressure-Lock syringe to reach a concentration of 200 ppmv. After kept for 15 min in dark environment, the glass vessel was irradiated from top by a 150 W xenon lamp (Hayashi UV410) which emits light of wavelength range of 350–400 nm at an intensity of 3.0 mW cm^{-2}. The degradation of acetaldehyde and the generation of carbon dioxide were monitored using a gas chromatograph (SP-2100A, BFRL Co.), equipped with a 2 m Porapak-Q column and a flame ionization detector.

The same method was used in visible-light irradiation (420 nm in wavelength and 119 mW cm^{-2} in intensity) to the degradation of acetaldehyde to check the photocatalytic activities of the samples.

3. Results and discussion

3.1. Characterizations of the catalysts synthesized

SEM images of silica nanosphere (used as template) and TiO_2@SiO_2 nanosphere, TEM image of TiO_2 hollow nanosphere and HRTEM image of Cu_xO–TiO_2 hollow nanosphere are shown in Fig. 1. It is found that the silica has regular ball-shape morphology with an average diameter about 25 nm (Fig. 1A). The average diameter of the microsphere increases to about 35 nm after TiO_2 framework formed on the surface (Fig. 1B). After immersed in NaOH solution (3.0 M) at 60 °C for 8.0 h, Si–O structure in TiO_2@SiO_2 nanosphere was damaged and the shell of TiO_2 remained. TEM image (Fig. 1C) indicates that final product has regular microspherical morphology with hollow structure, and its average diameter is about 35 nm. The shell thickness of these hollow microspheres is about several nanometers. HRTEM image (Fig. 1D) shows that there are Cu_xO clusters attached on the highly crystallized TiO_2 surfaces and formed clear lattice fringes. Particle size distributions of unmodified SiO_2 nanosphere, TiO_2@SiO_2 nanosphere and TiO_2 hollow nanosphere are also shown in Fig. 1.

The FT-IR spectra of SiO_2 nanosphere, TiO_2@SiO_2 nanosphere and TiO_2 hollow nanosphere are shown in Fig. 2. All the samples have stretching and bending vibrations absorptions of hydroxyl groups from surface of the samples and the adsorbed water, which are at 3400 and 1600 cm^{-1} respectively.[31] The antisymmetric stretching vibration absorption of Si–O–Si in SiO_2 (Fig. 2a) and TiO_2@SiO_2 nanospheres (Fig. 2b) are found at 1100 cm^{-1}, but it cannot be observed in Fig. 2c. Disappearance of Si–O–Si absorption in Fig. 2c indicates that there isn't any SiO_2 in the TiO_2 hollow nanosphere. Vibration absorption of Ti–O–Si in TiO_2@SiO_2 (Fig. 2b) is found at 960 cm^{-1},[32] indicating that the framework of $(Ti–O)_n$ was connected on the surface of silica gel after tetraethoxy titanium was adsorbed and hydrolyzed. At the same time, the absorptions of Ti–O in TiO_2@SiO_2 and TiO_2 hollow nanospheres are found at about 520 cm^{-1}.

EDS spectrum of TiO_2@SiO_2 nanosphere (Fig. 3A) shows that the nanosphere is consisted by Si (20.49%), Ti (7.86%) and O (71.65%) elements, proving the existence of both SiO_2 and TiO_2 frameworks in the sample. Calculation indicates that the proportion of TiO_2 and SiO_2 in TiO_2@SiO_2 nanosphere is about 1 : 3. However, only Ti and O elements are found in Fig. 3B, and the proportion of Ti and O is about 1 : 2, which confirms the removal of template and generation of TiO_2 hollow nanosphere.

The crystal phases of TiO_2 largely determines their suitabilities for photocatalytic activities.[33,34] The powder X-ray diffraction (PXRD) patterns of TiO_2@SiO_2 nanosphere and TiO_2 hollow nanospheres deposited by different concentrations of Cu^{2+} ions are shown in Fig. 4. Six characteristic peaks of anatase TiO_2 are observed at 25.2° (101), 37.8° (004), 48.1° (200), 53.9° (105), 56.1° (211) and 62.7° (204) in Cu_xO–TiO_2@SiO_2 nanospheres (Fig. 4A), which are indexed to diffractions of TiO_2 (ref. 35) except for the diffractions of SiO_2 at 21.79°. However, when the Cu content in the nanocomposite, diffraction peaks of two weak diffractions of Cu_xO (CuO and Cu_2O) were observed in 27.5° and 42.3°.[36] As to Cu_xO–TiO_2 hollow nanosphere (Fig. 4B), seven characteristic

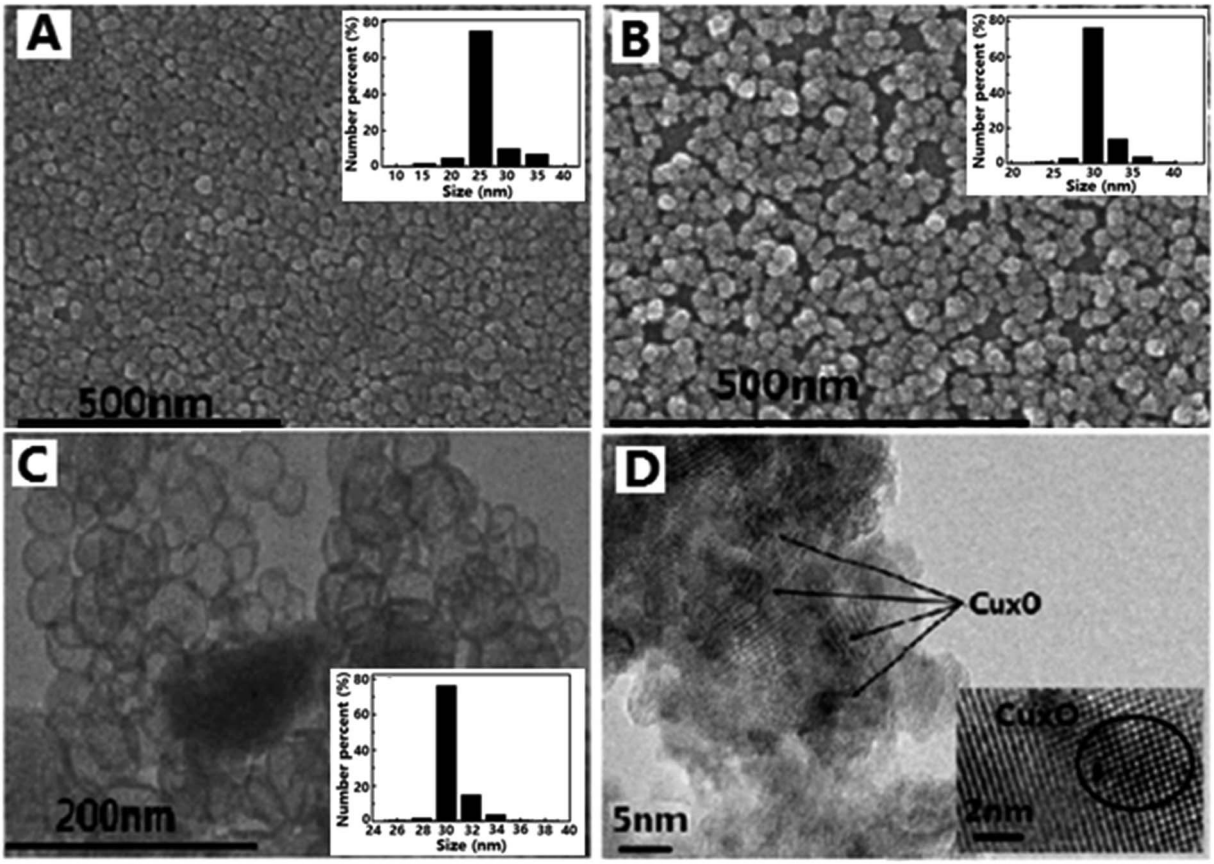

Fig. 1 SEM images and particle size distributions of unmodified SiO_2 (A) nanosphere and TiO_2@SiO_2 nanosphere (B); TEM image and particle size distribution of TiO_2 hollow nanosphere (C) and HRTEM image of Cu_xO–TiO_2 hollow nanosphere (D).

diffractions from anatase TiO_2 are observed, and all the diffractions are stronger than the corresponding diffractions in Cu_xO–TiO_2@SiO_2 nanosphere. Also the diffractions associated with Cu_2O at 27.5° and 42.3° on the surface of TiO_2 hollow nanosphere are found (Fig. 4B). All the results indicate that Cu_xO was attached to the surface of TiO_2, and the diffraction intensity from Cu_2O increases with its content. Elemental mapping analysis of the sample Cu_xO–TiO_2 hollow nanosphere (shown in Fig. S1 in the ESI†) indicates that the Cu element distributed uniformly though its content on TiO_2 surface was little.

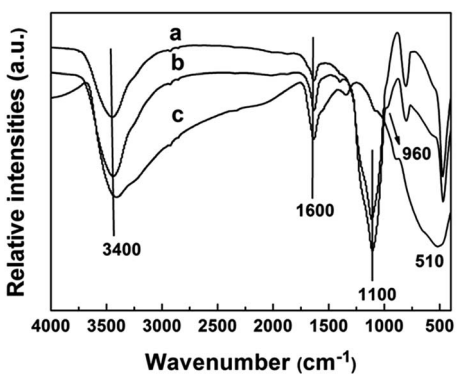

Fig. 2 FT-IR spectra of SiO_2 nanosphere (a), TiO_2@SiO_2 nanosphere (b) and TiO_2 hollow nanosphere (c).

Nitrogen adsorption–desorption isotherms of TiO_2@SiO_2 and TiO_2 hollow nanospheres are shown in Fig. 5. Isotherms exhibiting behavior between those of types I and IV are characteristic of mesopores, according to IUPAC classifications. In addition, the prepared TiO_2@SiO_2 nanosphere and TiO_2 hollow nanosphere own surface areas of 251 $m^2\ g^{-1}$ and 402 $m^2\ g^{-1}$, pore volumes of 0.613 $cm^3\ g^{-1}$ and 0.983 $cm^3\ g^{-1}$, respectively. These parameters are far more than those of P25 (49 $m^2\ g^{-1}$ of surface area and 0.090 $cm^3\ g^{-1}$ of pore volume), a kind of commercial TiO_2 microsphere.

In order to explore the chemical states of some relative elements in the nanocomposite samples, X-ray photoelectron spectroscopy (XPS) was carried out. In Fig. 6A, two peaks at 463.9 eV and 458.2 eV were observed from the Ti 2p spectrum, which are assigned to Ti $2p_{1/2}$ and Ti $2p_{3/2}$. No obvious differences were observed between the two spectra of TiO_2 and 0.5%-Cu_xO–TiO_2 hollow nanospheres, which indicate that Cu_xO was deposited on the surface of TiO_2 hollow nanospheres rather than the lattice. As shown in Fig. 6B, the appearance of CuO can be confirmed by the binding energies of 934.6 and 954.5 eV, respectively. There are another two characteristic peaks located at binding energies of 932.5 and 952.5 eV, which can be assigned to Cu(I) in Cu_2O.[37] Mole ratio of Cu^+ to Cu^{2+} is about

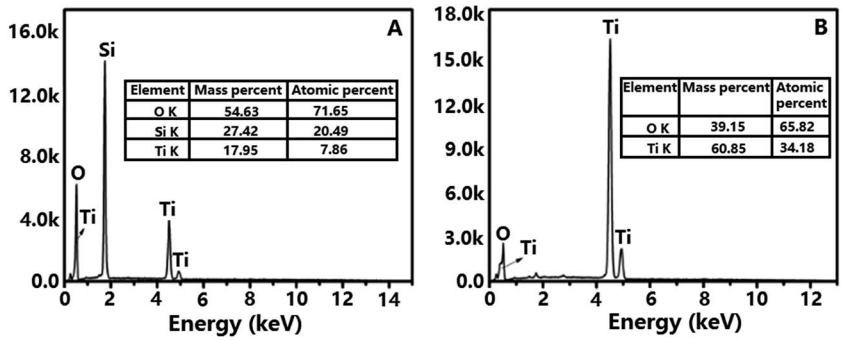

Fig. 3 EDS spectra of TiO_2@SiO_2 nanosphere (A) and TiO_2 hollow nanosphere (B).

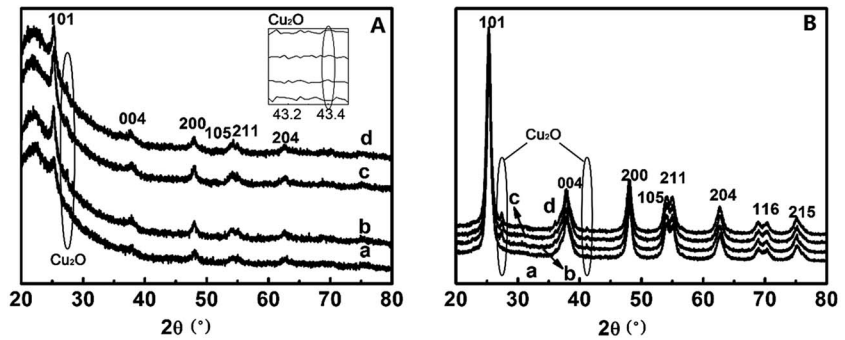

Fig. 4 (A) XRD patterns of TiO_2@SiO_2 nanospherical ((a) TiO_2@SiO_2; (b) 0.25%-Cu_xO–TiO_2@SiO_2; (c) 0.5%-Cu_xO–TiO_2@SiO_2; (d) 1.0%-Cu_xO–TiO_2@SiO_2); (B) XRD patterns of TiO_2 hollow nanospherical materials ((a) TiO_2 hollow sphere; (b) 0.25%-Cu_xO–TiO_2 hollow sphere; (c) 0.5%-Cu_xO–TiO_2 hollow sphere; (d) 1.0%-Cu_xO–TiO_2 hollow sphere).

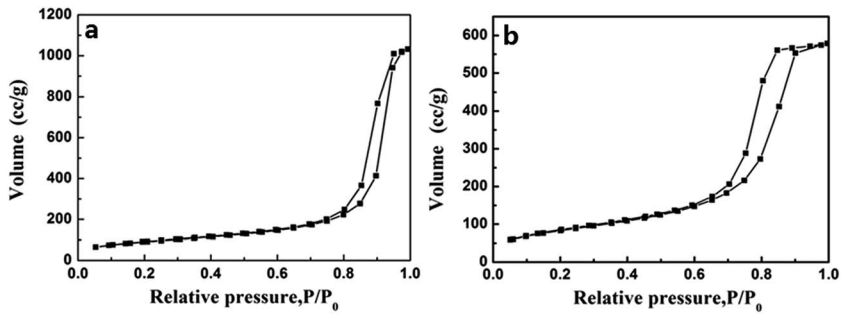

Fig. 5 The N_2 adsorption–desorption isotherms of TiO_2@SiO_2 nanosphere (a) and TiO_2 hollow nanosphere (b).

1.6 : 1, which calculated from the peak area in Fig. 6B. In process of the reaction, the hydrated Cu^{2+} ions were firstly adsorbed on the surface of TiO_2 hollow nanospheres. Some of Cu^{2+} ions were hydrolyzed to $Cu(OH)_2$ in this system, and later they were changed into CuO under a certain temperature (110 °C). Due to the semiconductive property, the electron–holes in TiO_2 would be separated under illumination of UV-light in the sunshine, and the electrons separated would be transferred to Cu(II) to form Cu_2O.

UV-Vis absorption spectra (shown in Fig. 7) indicate that all the samples, including TiO_2@SiO_2 nanosphere, TiO_2 hollow nanosphere, Cu_xO–TiO_2@SiO_2 nanosphere and Cu_xO–TiO_2 hollow nanosphere, have the intrinsic interband absorptions of TiO_2 at about 400 nm. The weak absorptions in range of 400–500 nm are assigned to the interfacial charge transfer in Cu_xO–TiO_2@SiO_2 nanosphere and Cu_xO–TiO_2 hollow nanosphere. In addition, the absorptions from 600 to 800 nm in the spectra of Cu_xO–TiO_2@SiO_2 nanosphere and Cu_xO–TiO_2 hollow nanosphere are assigned to the intrinsic excitation band of Cu_xO and the d–d transition of Cu(II).[33] Sequence of absorption intensities in range of 500–800 nm of the relative materials is TiO_2@SiO_2 nanosphere ≅ TiO_2 hollow nanosphere < Cu_xO–TiO_2@SiO_2 nanosphere < Cu_xO–TiO_2 hollow nanosphere, indicating that the Cu^{2+} ions on the surface of TiO_2 strengthen the absorption of the host in visible-light region, and the intensified degree on the absorptions increases with the increasing contents of Cu

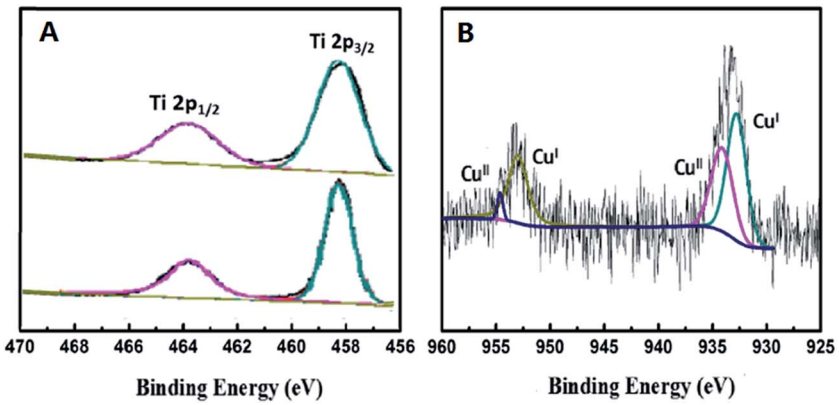

Fig. 6 XPS analysis of Ti 2p in TiO_2 hollow nanosphere (A) and Cu 2p in 0.5%-Cu_xO–TiO_2 hollow nanosphere (B).

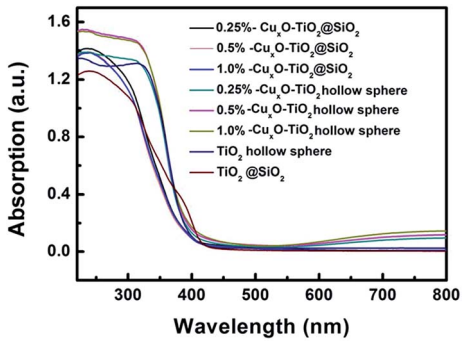

Fig. 7 UV-Vis absorption spectra of TiO_2@SiO_2, TiO_2 hollow nanosphere and Cu_xO–TiO_2@SiO_2 and Cu_xO–TiO_2 hollow nanospheres.

element in the composite materials, especially to TiO_2 hollow nanosphere.

3.2. Studies on catalytic activities of the catalysts

Photocatalytic activities of the catalysts were evaluated by monitoring degradation of acetaldehyde under UV-light and visible-light irradiations, and the initial concentration of acetaldehyde gas in all the experiments is about 200 ppmv. The first is to check the activities of the catalysts in a dark environment without any light irradiation. It was found that the concentration of acetaldehyde was almost not changed except for a little amount of acetaldehyde adsorbed (less than 20% of acetaldehyde adsorbed and less than 5% of CO_2 produced, which could be found from Fig. 8), which means that the acetaldehyde was not decomposed in dark under existence of the catalysts. However, the degradation of acetaldehyde happened when the reactor was irradiated by UV-light or visible-light, and large amount of CO_2 generated at the same time. Fig. 8 and 9 display the degradation of acetaldehyde and the generation of CO_2 in the systems under UV-light and visible-light irradiations, respectively. As shown in Fig. 8, the catalytic performance of TiO_2 hollow nanosphere was superior to TiO_2@SiO_2 nanosphere. Also it was found that the content of copper on the surface of TiO_2 affected the activities of catalysts deeply. The catalytic efficiency of 0.5%-Cu_xO–TiO_2 hollow nanosphere is higher than that of 0.25%-Cu_xO–TiO_2 hollow nanosphere. When the copper content is up to 0.5%, increase on catalytic efficiency of the hollow nanosphere is not evident. The above-mentioned regularity can be also found in the Cu_xO–TiO_2@SiO_2 nanospherical system. The decomposed rate of acetaldehyde by different catalysts under UV-light irradiation can be calculated by amount of the residual acetaldehyde and the generated CO_2. In the system of 0.5%-Cu_xO–TiO_2 hollow nanosphere, about 99.72–99.74% acetaldehyde was degraded

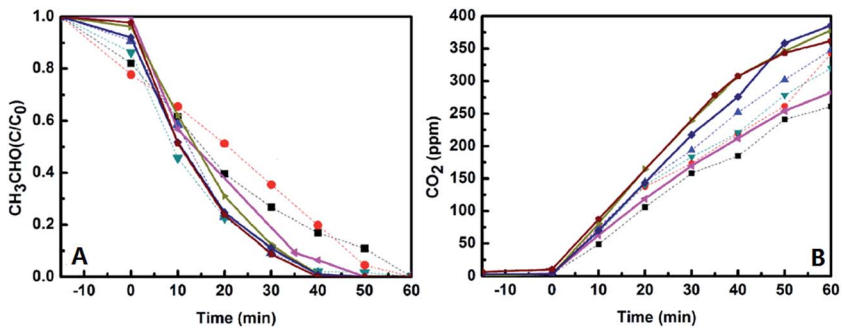

Fig. 8 Degradation of acetaldehyde with the variation of times (A) and amount of CO_2 generated (B) under UV light irradiation and existence of the catalysts (■: TiO_2@SiO_2; ●: 0.25%-Cu_xO–TiO_2@SiO_2; ▲: 0.5%-Cu_xO–TiO_2@SiO_2; ▼: 1.0%-Cu_xO–TiO_2@SiO_2; ◀: TiO_2 hollow sphere; ▶: 0.25%-Cu_xO–TiO_2 hollow sphere; ♦: 0.5%-Cu_xO–TiO_2 hollow sphere; ⬟: 1.0%-Cu_xO–TiO_2 hollow sphere).

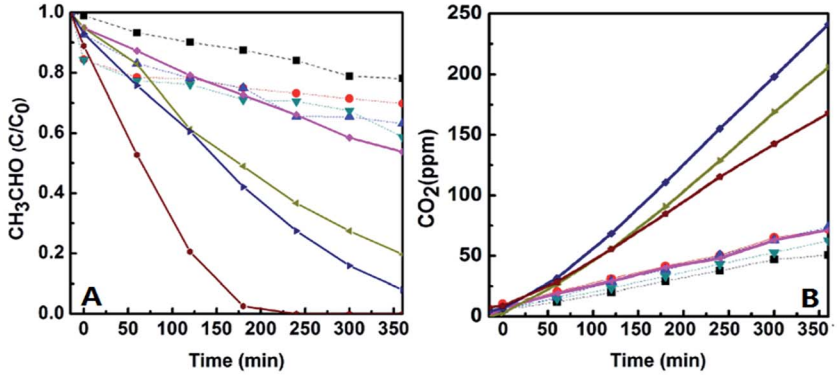

Fig. 9 Degradation of acetaldehyde with the variation of times (A) and amount of CO_2 generated (B) under visible light irradiation and existence of the catalysts (■: TiO_2@SiO_2; ●: 0.25%-Cu_xO–TiO_2@SiO_2; ▲: 0.5%-Cu_xO–TiO_2@SiO_2; ▼: 1.0%-Cu_xO–TiO_2@SiO_2; ◀: TiO_2 hollow sphere; ▶: 0.25%-Cu_xO–TiO_2 hollow sphere; ♦: 0.5%-Cu_xO–TiO_2 hollow sphere; ⬟: 1.0%-Cu_xO–TiO_2 hollow sphere).

after 60 minutes. Some data relating to degradation efficiency of acetaldehyde under UV-light and visible-light irradiations catalyzed by the relative catalysts are list in Tables 1 and 2. The clearance ratio is specific value of practical production and theoretical yield of CO_2.

Meanwhile, degradations of acetaldehyde irradiated under visible-light under the catalysts were studied, which are shown in Fig. 9. Little CO_2 generated from degradation of acetaldehyde under the existence of TiO_2@SiO_2 nanosphere and TiO_2 hollow nanosphere for the wide band gap of TiO_2. However in Cu_xO–TiO_2 hollow nanospherical systems, acetaldehyde could be degraded to CO_2 commendably despite of the efficiencies lower than in UV-light. There is about 62.77–62.79% acetaldehyde was degraded in 0.5%-Cu_xO–TiO_2 hollow nanosphere catalytic system, and the catalyst exhibits the best catalytic performance among all the catalysts. Only 20.52–20.54% of acetaldehyde was degraded in 0.5%-Cu_xO–TiO_2@SiO_2 nanosphere catalytic system. Concentration of CO_2 generated in 0.5%-Cu_xO–TiO_2 hollow nanosphere system reached 241 ppm after 6 h, which is more than three times to the CO_2 generated in Cu_xO–TiO_2@SiO_2 nanosphere system (74 ppm) in the same time. Such high degradation efficiency of acetaldehyde under visible-light irradiation was seldom reported.

Photocatalytic reaction under existence of the semiconductor is a complicated phenomenon. It includes light absorption, stimulation and transference of the carrier and redox reaction on the catalyst surface. Position of energy band determined by the electronic structure in the semiconductor is one of the main controlling factors on photocatalytic activity, which affects range of the light wavelength on catalyst responsibility directly. The visible-light is considered to initiate interfacial charge transfer. Electrons in the valence band (VB) of TiO_2 are directly transferred to Cu(II) to form Cu(I), as well as holes (h^+) in the VB of TiO_2. Thus, the energy to separate electrons and holes becomes low, which narrows the band gap of TiO_2 and prolongs the absorption edge from UV-light to visible-light

Table 1 Initial concentration of acetaldehyde, the amount of CO_2 generated and decomposed rate of acetaldehyde after 60 minutes under UV light irradiation (THN: TiO_2 hollow nanosphere, TS: TiO_2@SiO_2)

Sample	TS	0.25% Cu_xO–TS	0.5% Cu_xO–TS	1.0% Cu_xO–ST	THN	0.25% Cu_xO–THN	0.50% Cu_xO–THN	1.0% Cu_xO–THN
C_{CH_3CHO} (ppmv)	193.611	194.139	181.5	193.842	180.361	199.796	193.545	186.103
C_{CO_2} (ppmv)	260.989	342.129	347.763	319.558	282.625	378.431	386.044	361.759
Decomposed rate (%)	67.39–67.41	88.10–88.12	95.78–95.80	82.42–82.44	78.17–78.19	94.69–94.71	99.72–99.74	97.19–97.21

Table 2 Initial concentration of acetaldehyde, the amount of CO_2 generated and decomposed rate of acetaldehyde after 6 hours under visible light irradiation (THN: TiO_2 hollow nanosphere, TS: TiO_2@SiO_2)

Sample	TS	0.25%- Cu_xO–TS	0.5%- Cu_xO–TS	1.0%- Cu_xO–TS	THN	0.25%- Cu_xO–THN	0.5%- Cu_xO–THN	1.0%- Cu_xO–THN
C_{CH_3CHO} (ppmv)	197.620	179.355	180.328	183.991	174.042	178.035	192.159	200.409
C_{CO_2} (ppmv)	50.635	71.583	74.029	62.534	71.488	205.675	241.276	168.007
Decomposed rate (%)	12.80–12.82	19.95–19.97	20.52–20.54	17.69–17.71	20.53–20.55	54.99–55.01	62.77–62.79	41.91–41.93

region. The holes produced in VB of TiO_2 decompose organic substances. The catalytic degradation mechanism of acetaldehyde is shown in the following equations:[38]

$$TiO_2 \rightarrow h^+ + e^-$$

$$h^+ + H_2O \rightarrow {}^{\bullet}OH + H^+$$

$$O_2 + e^- \rightarrow O^{2-}$$

$$CH_3CHO + O^{2-} \rightarrow CH_3CO^{\bullet} + HO_2^-$$

$$CH_3CHO + HO_2^- \rightarrow CH_3CO^- + H_2O_2$$

$$H_2O_2 + CH_3CO^{\bullet} \rightarrow CH_3COOH + {}^{\bullet}OH$$

$$CH_3CO^- + {}^{\bullet}OH \rightarrow CH_3COOH + e^-$$

$$CH_3COOH + 2H_2O + 8h^+ \rightarrow 2CO_2 + 10H^+$$

Due to the larger surface area and more exposed active sites, the catalytic activity of Cu_xO–TiO_2 hollow nanosphere is higher than that of the catalyst Cu_xO–TiO_2@SiO_2 nanosphere. Moreover, the separation of electrons and holes became easier with Cu^{2+} increased on the surface of TiO_2, and superior catalytic activity of the catalyst was exhibited.

4. Conclusions

In summary, four kinds of photocatalysts, TiO_2@SiO_2 nanosphere, TiO_2 hollow nanosphere, Cu_xO–TiO_2@SiO_2 nanosphere and Cu_xO–TiO_2 hollow nanosphere, were synthesized. All the materials were found to have good photocatalytic activities in degradation of acetaldehyde under UV-light irradiations. Compared with TiO_2@SiO_2 nanosphere, TiO_2 hollow nanosphere and Cu_xO–TiO_2@SiO_2 nanosphere, Cu_xO–TiO_2 hollow nanosphere was superior for being used as catalyst in degradation of acetaldehyde under visible-light irradiation. The impregnated Cu^{2+} ions on the surface of TiO_2 hollow nanosphere were possibly to enhance the separation of photogenerated charge carriers.

Conflict of interest

The authors declare no competing financial interest.

Acknowledgements

We thank the projects of National Natural Science Foundation of China (No. U1362113 and No. 21521005) and the PetroChina Co. Ltd. For financial support.

References

1 B. Peng, L. F. Tan, C. Dong, X. W. Meng and F. Q. Tang, *ACS Appl. Mater. Interfaces*, 2012, **4**, 96–101.
2 S. Sandoval, J. Yang, J. G. Alfaro, A. Liberman and M. Makale, *Chem. Mater.*, 2012, **24**, 4222–4230.
3 L. Li, Y. Chen, S. Jiao, Z. Fang, X. Liu and Y. Xu, *Mater. Des.*, 2016, **100**, 235–240.
4 S. Son, H. H. Sun, C. Kim, Y. Y. Ju and J. Jang, *ACS Appl. Mater. Interfaces*, 2013, **5**, 4815–4820.
5 T. Sreethawong, S. Ngamsinlapasathian and S. Yoshikawa, *J. Colloid Interface Sci.*, 2014, **430**, 184–192.
6 K. Nishizawa, E. Watanabe and M. Maeda, *Mater. Sci. Appl.*, 2014, **5**, 112–123.
7 F. Akira, X. Zhang and D. A. Tryk, *Surf. Sci. Rep.*, 2008, **63**, 515–582.
8 N. Guo, Y. M. Liang, S. Lan, L. Liu and G. J. Ji, *Appl. Surf. Sci.*, 2014, **305**, 562–574.
9 D. M. Chen, H. Zhu and X. Wang, *Appl. Surf. Sci.*, 2014, **319**, 158–166.
10 Z. N. Song, M. Fathizadeh, Y. Huang, K. H. Chu, Y. Yoon and L. Wang, *J. Membr. Sci.*, 2016, **510**, 72–78.
11 Y. Chi, Q. Yuan, Y. Li, L. Zhao, N. Li and X. Li, *J. Hazard. Mater.*, 2013, **262**, 404–411.
12 M. Strauss, M. Pastorello, F. A. Sigoli and J. M. Silva, *Appl. Surf. Sci.*, 2014, **319**, 151–157.
13 L. Jing, W. Jia, Y. Qu and Y. Luan, *Appl. Surf. Sci.*, 2009, **256**, 657–663.
14 K. J. A. Raj and B. Viswanathan, *Indian J. Chem.*, 2009, **48**, 1378–1382.
15 Y. Bessekhouad, D. Robert and J. V. Weber, *J. Photochem. Photobiol., A*, 2004, **163**, 569–580.
16 S. G. Kumar and L. G. Devi, *J. Phys. Chem. A*, 2011, **115**, 13211–13241.
17 H. Fang, V. Kambala, M. Srinivasan, D. Rajarathnam and R. Naidu, *Appl. Catal., A*, 2009, **359**, 25–40.
18 R. Liu, F. Ren, W. Su, P. He, C. Shen and L. Zhang, *Ceram. Int.*, 2015, **41**, 14615–14620.
19 Z. Song, M. Fathizadeh, Y. Huang, K. H. Chu, Y. Yoon and L. Wang, *J. Membr. Sci.*, 2016, **510**, 72–78.
20 S. Ullah, E. P. Ferreira-Neto, A. A. Pasa, C. C. J. Alcântara, J. J. S. Acuña and S. A. Bilmes, *Appl. Catal., B*, 2015, **179**, 333–343.
21 E. Pakdel and W. A. Daoud, *J. Colloid Interface Sci.*, 2013, **401**, 1–7.
22 G. K. Mor, K. Shankar, M. Paulose, O. K. Varghese and C. A. Grimes, *Nano Lett.*, 2006, **6**, 215–218.
23 R. Wang, X. Cai and F. Shen, *Ceram. Int.*, 2013, **39**, 9465–9470.
24 H. Song, S. You, T. Chen and X. Jia, *J. Mater. Sci.: Mater. Electron.*, 2015, **26**, 1–9.
25 M. Miyauchi, A. Nakajima, K. Hashimoto and T. Watanabe, *Adv. Mater.*, 2000, **1**, 1923–1927.
26 H. Irie, K. Kamiya, T. Shibanuma, S. Miura, D. A. Tryk and T. Yokoyama, *J. Phys. Chem. C*, 2009, **113**, 10761–10766.
27 J. Huang, S. Wang, Y. Zhao, X. Wang and S. Wang, *Catal. Commun.*, 2006, **7**, 1029–1034.
28 L. Gnanasekaran, R. Hemamalini and K. Ravichandran, *J. Saudi Chem. Soc.*, 2015, **19**, 589–594.
29 L. Gnanasekaran, R. Hemamalini, R. Saravanan, *et al.*, *J. Mol. Liq.*, 2016, **223**, 652–659.

30 Y. Kuroda, Y. Sakamoto and K. Kuroda, *J. Am. Chem. Soc.*, 2012, **134**, 8684–8692.
31 L. Zhang, Z. Xing, H. Zhang, Z. Li, X. Wu and X. Zhang, *Appl. Catal., B*, 2016, **180**, 521–529.
32 L. Wu, Y. Zhou, W. Nie, L. Song and P. Chen, *Appl. Surf. Sci.*, 2015, **351**, 320–326.
33 P. Zhang, Y. Yu, E. Wang, J. Wang, J. Yao and Y. Cao, *ACS Appl. Mater. Interfaces*, 2014, **6**, 4622–4629.
34 K. T. Kim, G. Ali, K. Y. Chung, C. S. Yoon, H. Yashiro and Y. K. Sun, *Nano Lett.*, 2014, **14**, 416–422.
35 S. A. Bakar and C. Ribeiro, *Appl. Surf. Sci.*, 2016, **377**, 121–133.
36 X. Qiu, M. Miyauchi, K. Sunada, M. Minoshima, M. Liu and Y. Lu, *ACS Nano*, 2011, **6**, 1609–1618.
37 Q. Hu, J. Huang, G. Li, J. Chen, Z. Zhang and Z. Deng, *Appl. Surf. Sci.*, 2016, **369**, 201–206.
38 P. Zhang, F. Liang, G. Yu, Q. Chen and W. Zhu, *J. Photochem. Photobiol., A*, 2003, **156**, 189–194.